JOURNAL OF SPACECRAFT AND ROCKETS
Vol. 40, No. 1, January–February 2003

Thermoelastic Analysis of a Kick Motor Nozzle Incorporating Spatially Reinforced Composites

Jae-Seok Yoo* and In-Hyun Cho†
Korea Aerospace Research Institute, Taejon 305-333, Republic of Korea
and
Chun-Gon Kim‡
Korea Advanced Institute of Science and Technology, Taejon 305-701, Republic of Korea

The mechanical and thermal properties of spatially reinforced composites are predicted using volume average and rules of mixture of the rods and matrix properties for stiffness, thermal conductivity, and coefficient of thermal expansion. The distribution of Young's modulus, thermal conductivity, and coefficient of thermal expansion for three-dimensional/four-dimensional spatially reinforced composites are demonstrated. The study examines the elastic behavior, the temperature distribution, and the thermoelastic behavior of a kick motor nozzle, which includes a carbon/carbon spatially reinforced composite as a throat part. The elastic deformation of the nozzle composed of three-dimensional carbon/carbon spatially reinforced composite shows asymmetry, whereas the elastic deformation of four-dimensional carbon/carbon spatially reinforced composite nozzle shows uniformity in the circumferential direction. The thermoelastic deformations of both the three- and four-dimensional spatially reinforced composite nozzles are uniform in the circumferential direction. The deformation of the three-dimensional spatially reinforced composite nozzle is slightly smaller than that of the four-dimensional spatially reinforced composite nozzle in the nozzle throat. Circumferential stress is the critical stress component of the kick motor nozzle.

Nomenclature

C_p	=	specific heat, J/kg · K
$[C]$	=	stiffness matrix in the global coordinate system, GPa
$[C]_c$	=	stiffness matrix of spatially reinforced composites (SRC), GPa
$[C]_{\text{iso}}$	=	stiffness matrix of an isotropic media, GPa
$[C'']$	=	stiffness matrix in the local coordinate system, GPa
d	=	diameter of a rod, mm
E_{ij}	=	Young's modulus, GPa
G_{ij}	=	shear modulus, GPa
$[K]$	=	coordinate transformation matrix
k_i	=	thermal conductivity, W/m K
$[k]_c$	=	thermal conductivity of SRC, W/m K
$[k'']_c$	=	thermal conductivity of SRC in arbitrary directions, W/m K
$[S]_c$	=	compliance matrix of SRC, GPa^{-1}
$[S'']_c$	=	compliance matrix of SRC in arbitrary directions, GPa^{-1}
$[T]$	=	coordinate transformation matrix
V_r	=	summation of volume fraction of each rod
VF_i	=	volume fraction of each rod
α_i	=	coefficient of thermal expansion (CTE), /°C
$[\alpha]_c$	=	CTE of SRC, /°C
$[\alpha'']_c$	=	CTE of SRC in arbitrary directions, /°C
ν_{ij}	=	Poisson's ratio
ρ	=	density, kg/m^3

I. Introduction

LAMINATED composites are weak in the out-of-plane material properties, although most laminated composites have high specific stiffness and strength in-plane. Spatially reinforced composites (SRC) include reinforcing rods in the thickness direction and potentially have better out-of-plane mechanical and thermal properties in comparison with laminated composites.

SRC can be classified into four types of preforms: woven, knitted, braided, and nonwoven performs. Among them, multiaxial nonwoven performs consisting of reinforcing rods and matrix are most suitable for thick-walled structures. Material properties of SRC are strongly dependent on the fiber architecture of the perform, and the fiber architecture is configured to satisfy the given design requirements by predicting material properties of the SRC. The application of SRC has been limited thus far for several reasons. One reason is the lack of appropriate tools for the prediction of the material properties of SRC. In other words, if the mechanical and thermal material properties of SRC can be predicted by analysis, the application of SRC would be far more extended.

There are a few analytical methods to predict the material properties of SRC. Byun et al.[1] and Byun[2] predicted the stiffness properties for two-step braided, plain and eight-harness satin weave composites using the volume average of the fiber and the matrix stiffness. Rajiv[3] and Rajiv et al.[4] introduced a yarn slice as a piece of plain weave. The mechanical properties of the plain weave were calculated using the volume average of the yarn slice stiffness matrix for the unit cell of the plain weave. Nayfeh and Hefzy[5,6] also predicted the effective mechanical properties using the stiffness volume average of discrete isotropic trusslike rod elements.

To predict the thermal conductivity of SRC, both prediction equations of Tsai[7] and of Hashin[8] are used. Teters and Kregers[9] determined that the upper limit of the coefficient of thermal expansion (CTE) can be obtained by the volume average method.

Analyses have also been conducted to determine the performance of carbon/carbon SRC in rocket nozzle designs. Mukherjee and Sinha[10] performed a thermostructural analysis for a multidirectional composite nozzle having rotational symmetry. A steady-state heat transfer analysis was performed to obtain a temperature distribution of the nozzle. As a result of thermoelastic analyses of carbon/carbon, SiC/6061 Al, and T75/Nickel, the carbon/carbon composite performed best. However, a rod is assumed to be isotropic even though the rod is transversely isotropic. Yoo et al.[11] predicted mechanical properties of SRC and studied the mechanical behavior of a kick motor nozzle, which is made of graphite, three-dimensional and four-dimensional SRC. Schmidt et al.[12] reported that

Received 10 June 2002; revision received 20 August 2002; accepted for publication 27 August 2002.

*Senior Researcher, Space Launch Vehicle Division, 45 O-eun-dong, Yusong-gu.
†Senior Researcher, Propulsion Division, 45 O-eun-dong, Yusong-gu.
‡Professor, Division of Aerospace Engineering, 373-1 Kusong-dong, Yusong-gu; cgkim@kaist.ac.kr. Senior Member AIAA.

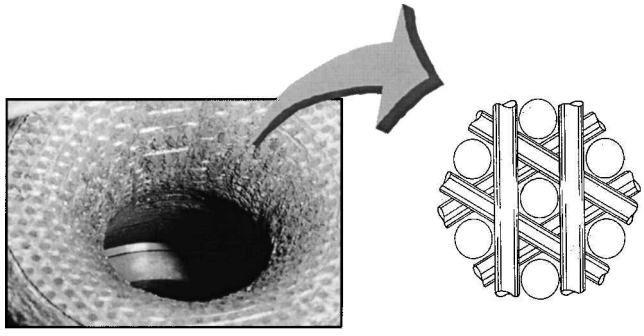

Four-dimensional SRC structure Four-dimensional SRC

Fig. 1 Spatially reinforced composite nozzle.

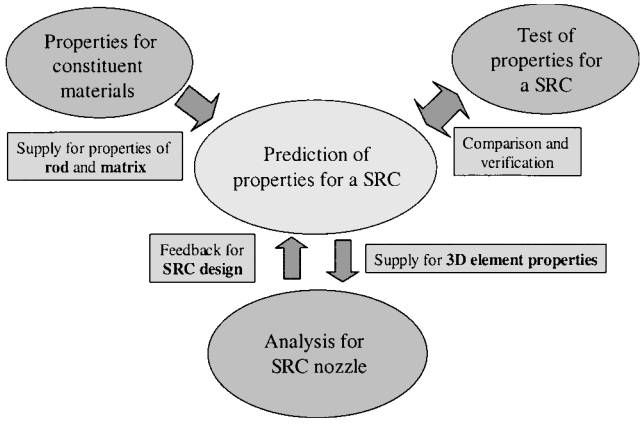

Fig. 2 Design procedure of SRC structures.

three-dimensional carbon/carbon SRCs are used in the integral throat-entrance section for the first stage nozzle of an intercontinental ballistic missile and the advanced solid rocket motor. Three qualification flight tests have been completed for the 5.4-t thrust solid propellant boosters.

A nozzle throat part is a typical application of thick-walled nonwoven SRC, which is usually made of carbon/carbon composites, as shown in Fig. 1. If the dimension of the nozzle throat varies with pressure and temperature, it will be difficult to control a rocket due to the change in the thrust vector. The dimensional stability of the nozzle throat can be ensured by the proper selection of an SRC architecture. From this viewpoint of dimensional stability, the thermo- elastic analysis is needed for the nozzle throat because it is directly connected to the deformation of the nozzle throat. Because the nozzle throat section is made of SRC, a material property prediction program for SRC becomes necessary. To date, there are few studies on the application of this SRC.

Figure 2 shows the total design procedure of SRC structures. The constituent materials properties of the rod and matrix are required to predict the material properties of SRC. The rod and matrix properties can be obtained from experiments and the prediction equations of a unidirectional composite[11] of a rod. To verify the predicted results of SRC, it is necessary to compare the experimental results with the results from analysis of SRC based on the predicted material properties. These predicted results provide three-dimensional material properties for SRC structures. Also, SRC architecture can be designed from the feedback of the SRC structures analysis.

In this paper, the equivalent mechanical and thermal properties of SRC are predicted using the superposition of mechanical and thermal properties of rods and matrix. Also, the spatial distribution of properties of SRC is demonstrated. The mechanical behavior, transient heat transfer, and thermoelastic behavior of a kick motor nozzle made of three-dimensional or four-dimensional SRC, carbon/phenolic and steel are studied using the transient thermoelastic finite element analysis. It is shown that a four-dimensional SRC nozzle, having diameters of [1,1,1,1.7] in each rod direction has the smallest circumferential stress among several SRC nozzles considered.

II. Prediction of Material Properties for SRC

Prediction of Mechanical Properties

Figure 3 shows the coordinate system of a spatially oriented rod. The local (or rod) coordinate system is designated as $1''$–$2''$–$3''$, where $1''$ coincides with the axial direction of the rod, and the global (or structural) coordinate system is indicated as 1–2–3. The coordinate transformation of stiffness and compliance matrices can be obtained through the coordinate transformation of stress and strain. The resultant equation of the coordinate transformation for the stiffness matrix can be derived as

$$[C] = [K]^T [C''][K] \tag{1}$$

where $[K]$ is represented as the following function of rotation angles ψ and ϕ of coordinates for the stiffness matrices and ψ and ϕ are described in Fig. 3:

$$[K] = \begin{bmatrix} m^2p^2 & m^2q^2 & n^2 & mnq & mnp & m^2pq \\ q^2 & p^2 & 0 & 0 & 0 & -pq \\ n^2p^2 & n^2q^2 & m^2 & -mnq & -mnp & n^2pq \\ 2npq & -2npq & 0 & mp & -mq & -n(p^2-q^2) \\ -2mnp^2 & -2mnq^2 & 2mn & (m^2-n^2)q & (m^2-n^2)p & -2mnpq \\ -2mpq & 2mpq & 0 & np & -nq & m(p^2-q^2) \end{bmatrix} \tag{2}$$

where $m = \cos\psi$, $n = \sin\psi$, $p = \cos\phi$, and $q = \sin\phi$.

$[C]$ is the stiffness matrix in the global coordinate system, and $[C'']$ is the stiffness matrix in the local coordinate system, which can be obtained from the relationship $[C''] = [S'']^{-1}$. $[S'']$ is the compliance matrix in the local coordinate system and is given by

$$[S''] = \begin{bmatrix} \frac{1}{E_{1r}} & -\frac{\nu_{12r}}{E_{1r}} & -\frac{\nu_{12r}}{E_{1r}} & 0 & 0 & 0 \\ -\frac{\nu_{12r}}{E_{1r}} & \frac{1}{E_{2r}} & -\frac{\nu_{32r}}{E_{2r}} & 0 & 0 & 0 \\ -\frac{\nu_{12r}}{E_{1r}} & -\frac{\nu_{32r}}{E_{2r}} & \frac{1}{E_{2r}} & 0 & 0 & 0 \\ 0 & 0 & 0 & \frac{1}{G_{23r}} & 0 & 0 \\ 0 & 0 & 0 & 0 & \frac{1}{G_{12r}} & 0 \\ 0 & 0 & 0 & 0 & 0 & \frac{1}{G_{12r}} \end{bmatrix} \tag{3}$$

Figures 4 and 5 show the unit cells of a three-dimensional and four-dimensional SRC, respectively. The unit cell is a generic composite block consisting of fiber material bonded to matrix material, and repetition of the unit cell constructs the whole SRC. The mechanical and thermal properties for these unit cells are calculated using the volume average of stiffness for rods and matrix. To aid in analyzing

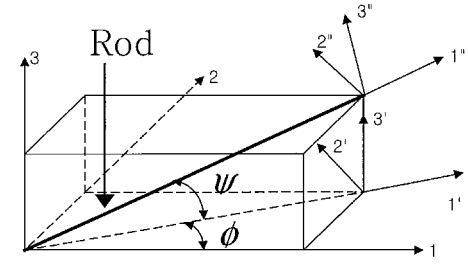

Fig. 3 Local and global coordinate system for the rod.

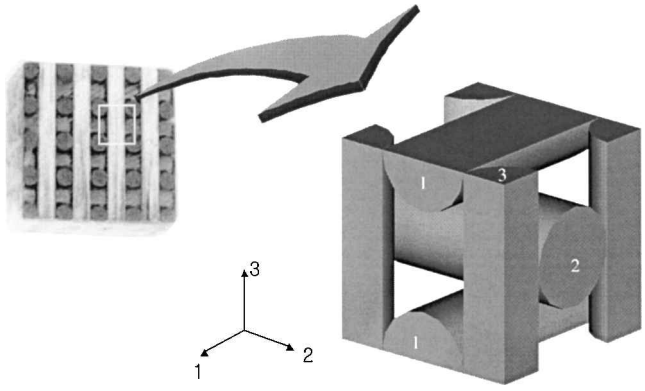

Fig. 4 Unit cell of the three-dimensional SRC.

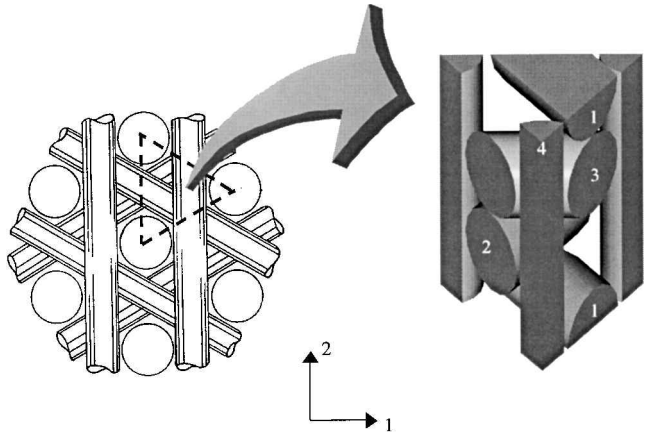

Fig. 5 Unit cell of the four-dimensional SRC.

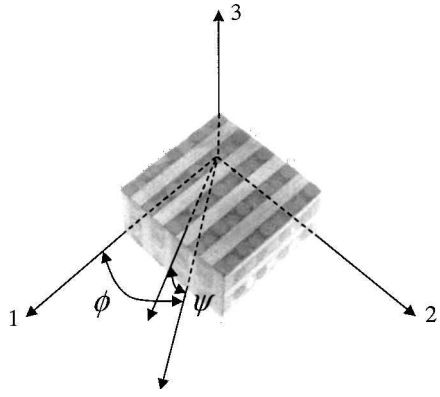

Fig. 6 Arbitrary direction of the SRC.

these unit cells, the volume fraction for each rod is defined as

$$\mathrm{VF}_i = \frac{i\text{th rod volume}}{\text{unit cell volume}} \begin{cases} i = 1, 2, 3 \text{ for three-dimensional SRC} \\ i = 1, 2, 3, 4 \text{ for four-dimensional SRC} \end{cases} \tag{4}$$

If the strain in the unit cell is constant, that is, an isostrain state,[1–4] it is possible to superpose the stiffness matrix of rods and matrix. This assumption is true if the SRC is about 10 or more times larger than the unit cell and there is no separation between the rods and matrix. With the isostrain assumption, the stiffness matrix of the unit cell of SRC is obtained by the superposition of the stiffness matrix of rods and matrix:

$$[C]_c = \sum_{i=1}^{n} \mathrm{VF}_i [K]_i^T [C''][K]_i + \left(1 - \sum_{i=1}^{n} \mathrm{VF}_i\right)[C]_{\mathrm{iso}} \tag{5}$$

where $n = 3$ or $n = 4$ correspond to the three-dimensional SRC or the four-dimensional SRC, respectively. $[C]_{\mathrm{iso}}$ is the stiffness matrix of isotropic media, and $[C]_c$ is the stiffness matrix of the unit cell for the SRC and provides three-dimensional composite stiffness properties to a nozzle throat composed of the SRC.

The compliance matrix of the unit cell for the SRC can be obtained by the inversion of the stiffness matrix for the unit cell of the SRC ($[S]_c = [C]_c^{-1}$). The material properties of the SRC in the global coordinate system as shown in Fig. 6 can be obtained from the compliance components as

$$\begin{aligned} E_{11c} &= 1/S_{11c}, & E_{22c} &= 1/S_{22c}, & E_{33c} &= 1/S_{33c} \\ G_{23c} &= 1/S_{44c}, & G_{31c} &= 1/S_{55c}, & G_{12c} &= 1/S_{66c} \\ \nu_{12c} &= -S_{21c}/S_{11c}, & \nu_{31c} &= -S_{13c}/S_{33c}, & \nu_{23c} &= -S_{32c}/S_{22c} \end{aligned} \tag{6}$$

The mechanical properties of an SRC in arbitrary directions can be given using the coordinate transformation of the compliance matrix for the SRC. The three-dimensional distributions of material properties for SRC are calculated using

$$[S'']_c = [K][S]_c[K]^T \tag{7}$$

As shown in Figs. 4 and 5, three-dimensional and four-dimensional SRC have spatially symmetric shapes. Therefore, the compliance matrix of SRC is calculated for ϕ and ψ from 0 to 90 deg at a 3-deg intervals in Figs. 4 and 5. Because SRC consists of rods and matrix, the constituent material properties of the rod and matrix are required to predict the material properties of SRC. The material properties of a reinforcing rod that makes the nonwoven preform of SRC need to be determined first. The rods for the SRC preform are pultruded T300 carbon fiber/epoxy, but the matrix of the rods and the infiltrated matrix of the preform are charred and carbonized to make the final thick-walled carbon/carbon composites. Therefore, it is very hard to measure the properties of the rod without the carbon matrix for carbon/carbon composites. A T300 carbon fiber[13] and carbon matrix[14] are used to constitute the carbon/carbon composites. The material properties of the T300 carbon fiber and the carbon matrix are shown in Table 1. From these material properties, the mechanical and thermal properties of a T300/carbon rod can be estimated by using the unidirectional composite prediction equations of Chamis[13] and Hashin,[8] respectively. The material properties of the rod are listed in Table 2.

The distribution of the tensile modulus for the three-dimensional SRC is shown in Fig. 7. The tensile modulus in each rod direction

Table 1 Material properties of the T300 carbon fiber

Symbol	T300 carbon fiber	Carbon matrix
E_1, GPa	220.6	3
E_2, GPa	13.79	3
G_{12}, GPa	8.964	1.11
G_{23}, GPa	4.827	1.11
ν_{12}	0.2	0.35
k_1, W/mK	8.365	25
k_2, W/mK	0.8365	25
α_1, $\times 10^{-6}/^{\circ}$C	−0.99	4
α_2, $\times 10^{-6}/^{\circ}$C	10.08	4

Table 2 Calculated material properties of the rod (fiber volume fraction = 0.66)

Symbol	T300/carbon
E_{1r}, GPa	146.7
E_{2r}, GPa	7.52
G_{12r}, GPa	5.21
G_{23r}, GPa	2.55
ν_{12r}	0.245
k_{1r}, W/mK	14.02
k_{2r}, W/mK	5.92
α_{1r}, $\times 10^{-6}/^{\circ}$C	−0.96
α_{2r}, $\times 10^{-6}/^{\circ}$C	8.76

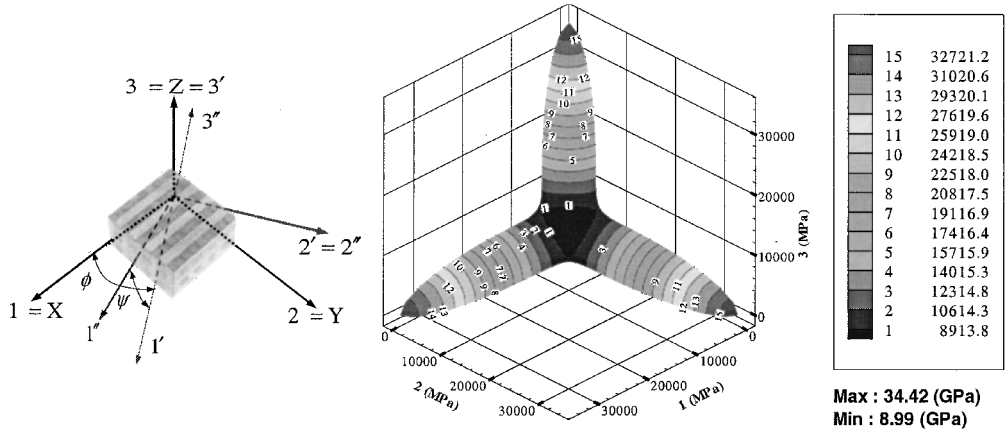

Fig. 7 Tensile modulus distribution of the three-dimensional SRC.

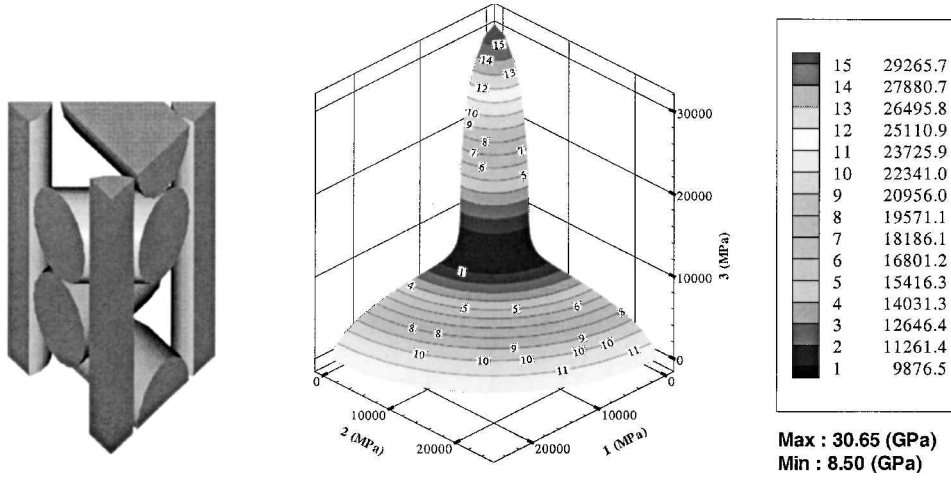

Fig. 8 Tensile modulus distribution of the four-dimensional SRC.

has the highest value. The tensile modulus, however, has the smallest value in the 45-deg rotated direction from the rod because the tensile modulus in that direction is mostly affected by the properties of the matrix, which are much smaller than those of the rod as shown in Tables 1 and 2.

Figure 8 shows the tensile modulus distribution of the four-dimensional SRC. The four-dimensional SRC has different property characteristics compared with those of the three-dimensional SRC. The four-dimensional SRC consist of 0-, 60-, and 120-deg rods in the 1–2 plane as shown in Fig. 5; therefore, the four-dimensional SRC has quasi-isotropic properties in the 1–2 plane, whereas the tensile modulus has the smallest value in the 45-deg rotated direction from the 1–2 plane, which is the maximum disoriented direction from each rod.

Prediction of Thermal Properties

The thermal conductivity and the CTE of SRC are also predicted by using the volume average of the thermal conductivity and the CTE of the rods and matrix. The equations to predict the thermal properties are

$$[k]_c = \sum_{i=1}^{n} \frac{\mathrm{VF}_i}{V_r}[K]_i^T[k''], \qquad [\alpha]_c = \sum_{i=1}^{n} \frac{\mathrm{VF}_i}{V_r}[K]_i^T[\alpha''] \quad (8)$$

where

$$V_r = \sum_{i=1}^{n} \mathrm{VF}_i$$

is the summation of the volume fraction of each rod. Thermal properties of rod and matrix are listed in Tables 1 and 2. The thermal properties of an SRC in arbitrary directions can be estimated using the coordinate transformation of the thermal conductivity and the CTE matrix:

$$[k'']_c = [T][k]_c, \qquad [\alpha'']_c = [T][\alpha]_c \quad (9)$$

where $[T]$ is defined as the following function of rotation angles of coordinates and ψ and ϕ are described in Fig. 3:

$$[T] = \begin{bmatrix} m^2p^2 & m^2q^2 & n^2 & 2mnq & 2mnp & 2m^2pq \\ q^2 & p^2 & 0 & 0 & 0 & -2pq \\ n^2p^2 & n^2q^2 & m^2 & -2mnq & -2mnp & 2n^2pq \\ npq & -npq & 0 & mp & -mq & -n(p^2-q^2) \\ -mnp^2 & -mnq^2 & mn & (m^2-n^2)q & (m^2-n^2)p & -2mnpq \\ -mpq & mpq & 0 & np & -nq & m(p^2-q^2) \end{bmatrix} \quad (10)$$

where $m = \cos\psi$, $n = \sin\psi$, $p = \cos\phi$, and $q = \sin\phi$.

The thermal conductivity distributions of the three-dimensional/four-dimensional SRC with the same rod diameter (1 mm) in each direction are shown in Fig. 9. The thermal conductivity distributions of the three-dimensional and four-dimensional SRC resemble an isotropic and transversely isotropic distribution. These distributions are not affected by off-rod properties of SRC, unlike the mechanical properties distribution of SRC. Because a principal axis of a thermal conductivity and CTE matrix exists, in which offdiagonal terms are zero. The CTE distributions of the

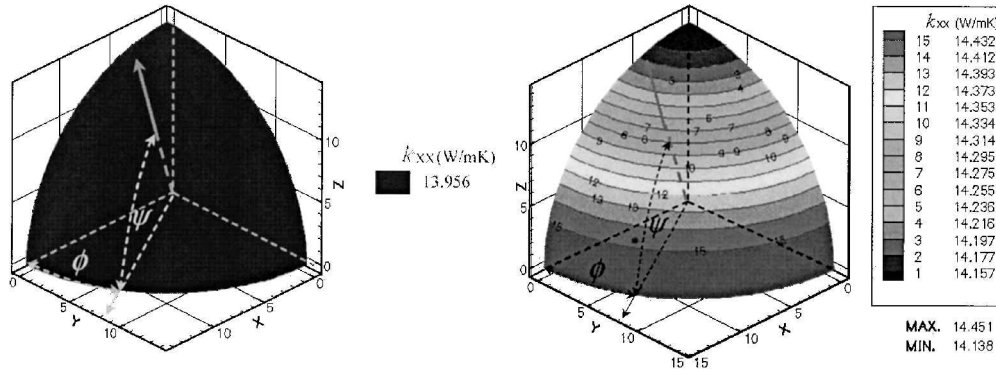

Three-dimensional SRC [1, 1, 1], mm Four-dimensional SRC [1, 1, 1, 1], mm

Fig. 9 Thermal conductivity distribution of the three-dimensional/four-dimensional SRC.

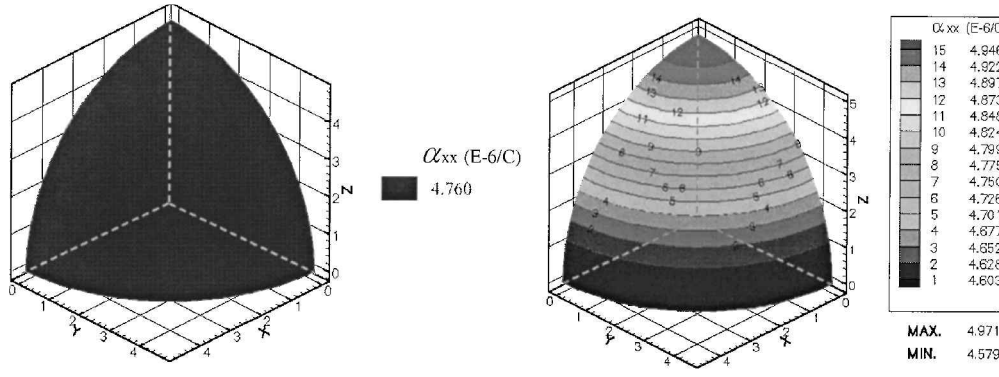

Three-dimensional SRC [1, 1, 1], mm Four-dimensional SRC [1, 1, 1, 1], mm

Fig. 10 CTE distribution of the three-dimensional/four-dimensional SRC.

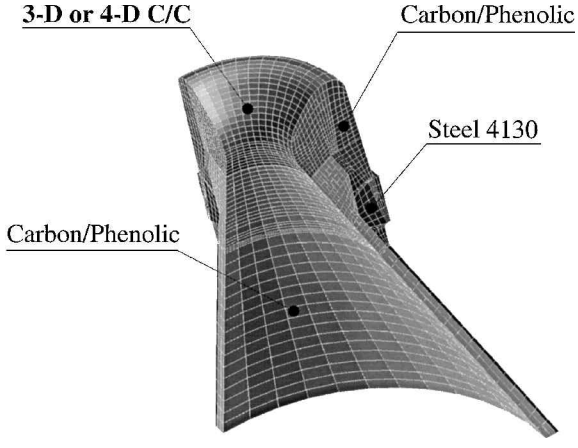

Fig. 11 Shape and constituent materials of a kick motor nozzle.

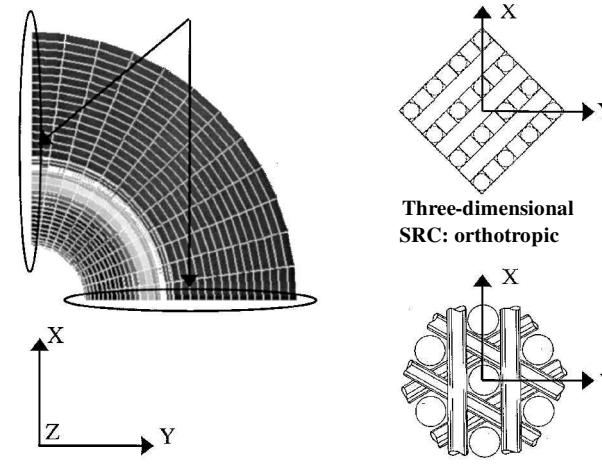

Fig. 12 Cyclic symmetry boundary condition on the nozzle.

three-dimensional/four-dimensional SRC are similar to the thermal conductivity distributions shown in Fig. 10.

III. Thermoelastic Analysis of the Kick Motor Nozzle

As shown in Fig. 11, the kick motor nozzle consists of the three-dimensional or the four-dimensional carbon/carbon SRC as the nozzle throat, carbon/phenolic as the outer surface of the nozzle entrance and the inner surface of the expansion part, and steel as the outer surface of the expansion part. For this kick motor nozzle, several factors are examined: elastic analysis to estimate the effects of the pressure, heat transfer analysis to obtain the temperature distribution of kick motor nozzle, and thermoelastic analysis to estimate the effects of the pressure and temperature using finite element analysis. In the finite element analysis, three-dimensional solid elements are used, which have eight nodes. The total numbers of elements and nodes are 6672 and 8086, respectively. MSC/PATRAN was used as the pre- and postprocessor, and ABAQUS was the analysis code.

Boundary Conditions and Material Properties

A cyclic symmetry boundary condition is applied to the kick motor nozzle for an effective analysis. The three-dimensional SRC has the 90-deg cyclic symmetric angle, as shown in Fig. 12. Therefore, only one-quarter of the kick motor nozzle is modeled. The four-dimensional SRC has a 60-deg cyclic symmetric angle; however, due to the quasi-isotropy in the X–Y plane of the four-dimensional SRC, it does not matter how large the angle of cyclic symmetry is in the X–Y plane. Hence, one-quarter of the nozzle is modeled for the four-dimensional SRC also.

Table 3 Material properties of the nozzle throat part

Symbol	Carbon/carbon			
	Three dimensional	Three dimensional	Four dimensional	Four dimensional
$[d_1, d_2, d_3, (d_4)]$, mm	[1,1,1]	[1,1,1.7]	[1,1,1,1]	[1,1,1,1.7]
$E_{11} = E_{22}$, GPa	34.42	27.43	24.60	19.84
E_{33}, GPa	34.42	50.31	30.65	44.33
G_{12}, GPa	2.552	2.487	9.17	7.350
$G_{13} = G_{23}$, GPa	2.552	2.634	2.48	2.519
ν_{12}	0.0830	0.109	0.341	0.349
$\nu_{23} = \nu_{13}$	0.0830	0.0551	0.0664	0.0451
$k_1 = k_2$, W/mK	13.96	13.13	14.45	13.89
k_3, W/mK	13.96	15.04	14.14	15.37
$\alpha_1 = \alpha_2$, $\times 10^{-6}/^\circ$C	4.76	5.56	4.58	5.32
α_3, $\times 10^{-6}/^\circ$C	4.76	3.22	4.97	3.46
C_p, J/kg · K	1153	1149	1159	1160
ρ, kg/m^3	1514	1518	1507	1506

Table 4 Material properties of the carbon/phenolic and steel of the nozzle

Symbol	Carbon/phenolic[a]	Steel 4130[b]
$E_{11} = E_{22}$, GPa	74.5[c]	205 (Ref. 17)
E_{33}, GPa	15.71 (Ref. 2)	205 (Ref. 17)
G_{12}, GPa	5.017[d]	78.13
$G_{13} = G_{23}$, GPa	4.65 (Ref. 2)	78.13
ν_{12}	0.1[c]	0.28 (Ref. 17)
$\nu_{23} = \nu_{13}$	0.54, (Ref. 2)	0.28 (Ref. 17)
$k_1 = k_2$, W/mK	2.38 (Ref. 15)	40.6 (Ref. 17)
k_3, W/mK	0.38 (Ref. 15)	40.6 (Ref. 17)
$\alpha_1 = \alpha_2$, $\times 10^{-6}/^\circ$C	−1.5 (Ref. 16)	14.6 (Ref. 17)
α_3, $\times 10^{-6}/^\circ$C	27 (Ref. 16)	14.6 (Ref. 17)
C_p, J/kg · K	1206	595
ρ, kg/m^3	1329	7800

[a]For carbon/phenolic, 1–2–3 axis = θ–Z–r axis (cylindrical coordinate).
[b]For steel, 1–2–3 axis = X–Y–Z axis (Cartesian coordinate).
[c]Obtained from experiments. [d]Calculated from the ±45-deg carbon/phenolic test results and the experimental values.

All of the degrees of freedom in the connecting part of the nozzle and combustion chamber are fixed. The connecting part is supposed to be an adiabatic state due to cutting off the heat by the carbon/phenolic composite in the entrance part and insulation material inside of the combustion chamber. Actually, the temperature of the connecting part is not very high, which was confirmed by the operational tests of the nozzle; therefore, the adiabatic state of the connecting part is an acceptable assumption. The outside of steel diverging part is estimated to be at room temperature. The material properties of the three-dimensional/four-dimensional SRCs were calculated from Eqs. (6) and (8) and are listed in Table 3. The specific heat and density of the three-dimensional/four-dimensional SRC in Table 3 were obtained by using the rule of mixture of a rod and matrix. The three-axis in Table 3 denotes the axial direction of the kick motor nozzle. The material properties of carbon/phenolic listed in Table 4 (Refs. 2 and 15–17), were obtained from experimental measurements and predictions of material properties of textile composites using the volume average of the stiffness and compliance matrix of unit cell and warp or fill yarn where there is an undulated region, respectively.[1,2]

Loading condition

Figure 13 shows the pressure distribution on the inner wall along the axisymmetric axis of the kick motor nozzle. This pressure distribution supplied by Korea Aerospace Research Institute (KARI) represents the steady state on a full scale. The wall pressure in Fig. 13 is high from the entrance to the throat. However, the wall pressure rapidly decreases in the expansion part due to an increment of the cross-sectional area of the nozzle. Figure 14 shows the temperature distribution on the wall in a steady-state condition. The temperature distribution of the combustion gas is also supplied by KARI. However, there are differences between the combustion gas

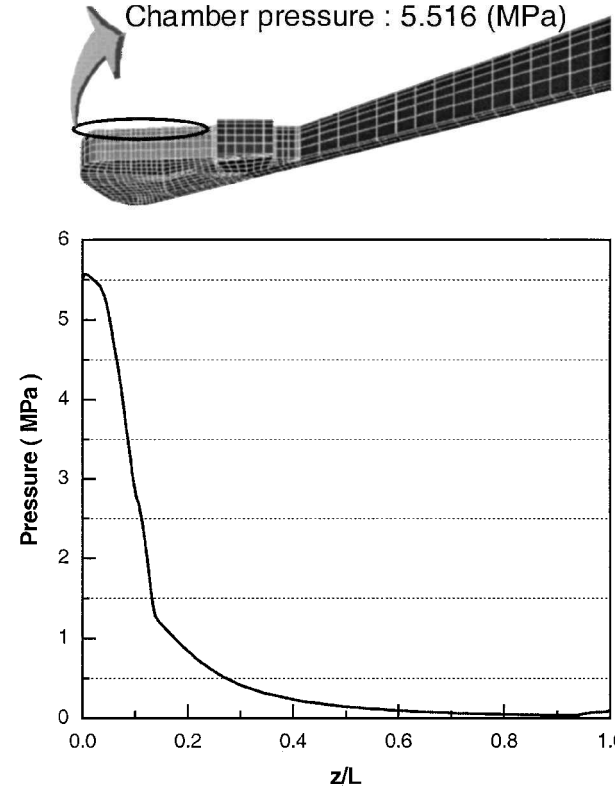

Fig. 13 Pressure distribution on the wall along the axis.

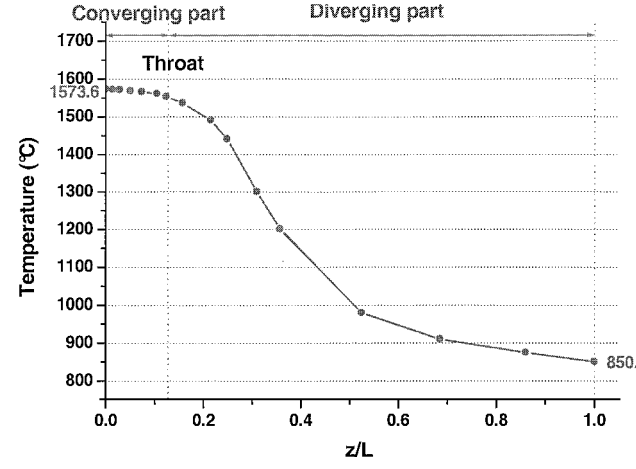

Fig. 14 Temperature distribution on the wall along the axis.

and the wall temperature. Therefore, the temperature distribution on the wall is obtained from the ratio of the combustion gas and the wall temperature.[10] Because the outer surface of the nozzle throat is inserted into a combustion chamber, there is no flow on the outer surface of the nozzle throat. Therefore, the chamber pressure and the temperature are the constant value, which are 5.516 MPa and 1573.6°C, respectively.

Results and Discussion

The deformed shapes of the three-dimensional/four-dimensional SRC nozzles under the pressure load condition are shown in Fig. 15 when the pressure load is applied to the kick motor nozzle. The deformation of the kick motor nozzle as shown in Fig. 15 is exaggerated 200 times. Because the pressure on the outer surface of the nozzle entrance part is higher than the pressure on the inner surface, the nozzle throat part is deformed toward the inside of the nozzle axis. The maximum deformations of the three-dimensional/four-dimensional SRC nozzle are 0.0238 and 0.0226 mm and occur in the nose tip of the nozzle entrance. The deformation of the

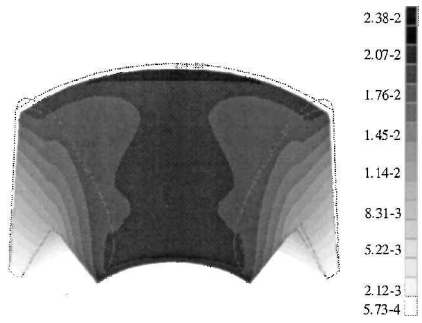

Three-dimensional SRC [1, 1, 1], mm, front view

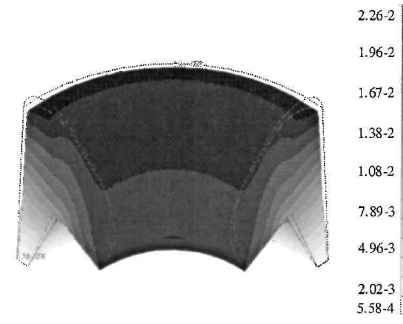

Four-dimensional SRC [1, 1, 1, 1], mm, front view

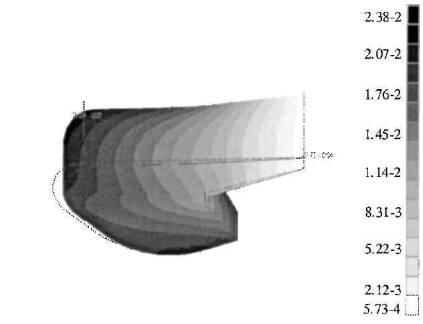

Three-dimensional SRC [1, 1, 1], mm, side view

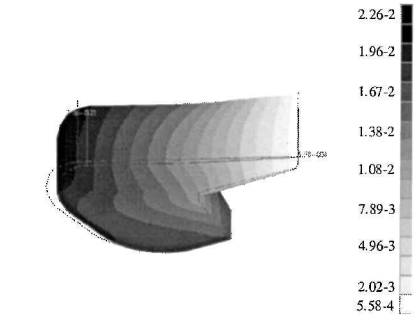

Four-dimensional SRC [1, 1, 1, 1], mm, side view

Fig. 15 Deformed shapes of the three-dimensional/four-dimensional SRC nozzles under pressure loading.

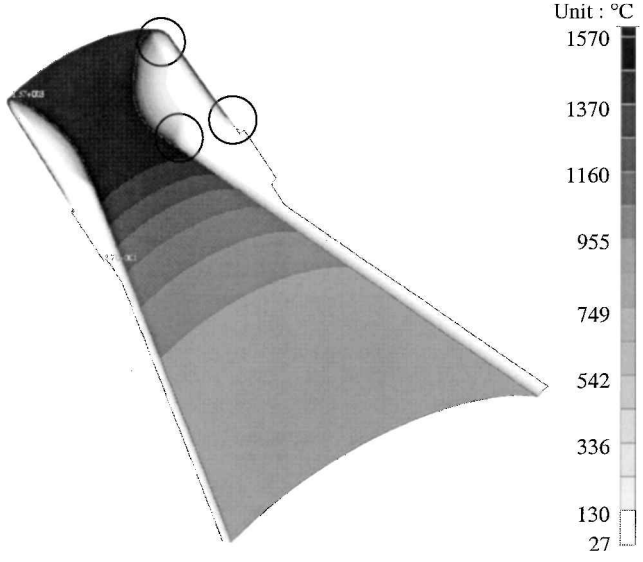

Fig. 16 Temperature distribution of the four-dimensional SRC at the final burning time of 9 s.

four-dimensional SRC nozzle is more uniform than the three-dimensional SRC nozzle due to the anisotropy of three-dimensional SRC in X–Y plane (Fig. 12).

The transient heat transfer analysis was performed on several three-dimensional/four-dimensional SRC nozzles to get the temperature distribution of the kick motor nozzle vs time. Figure 16 shows the temperature distribution at a final burning time of 9 s. The temperature distribution shows the isotropic characteristics in the circumferential direction of the nozzle because the thermal conductivity of three-dimensional/four-dimensional SRC is isotopic or transversely isotropic. The thermal gradient of each connecting part is shown to be high in Fig. 16, which induces a high stress concentration in each connecting part.

The thermoelastic analysis considered the temperature distribution from the transient heat transfer analysis at the final burning time and the pressure distribution in Fig. 13, simultaneously. The deformation of the kick motor nozzle as shown in Fig. 17 is exaggerated 10 times. The maximum deformation of the four-dimensional SRC nozzle having diameters of [1,1,1,1] in each direction is slightly smaller than that of the three-dimensional SRC nozzle. However, the more important deformation is in the nozzle throat, which has a direct effect on the rocket thrust. Table 5 shows the deformations of the nozzle throat for the three-dimensional/four-dimensional SRC nozzles having diameters of [1,1,1 mm], [1,1,1.7 mm], [1,1,1,1 mm], and [1,1,1,1.7 mm] in each direction, respectively. (The direction of the last rod is the Z direction in Fig. 12.)

Table 5 Deformation of the nozzle throat

Nozzle [mm]	Rod direction, mm	45-deg rotated direction, mm
Three dimensional [1,1,1]	0.244	0.240
Three dimensional [1,1,1.7]	0.223	0.219
Four dimensional [1,1,1,1]	0.258	0.257
Four dimensional [1,1,1,1.7]	0.250	0.250

The three-dimensional SRC nozzle has a smaller deformation in the nozzle throat in comparison with the four-dimensional SRC; however, the deformation of the four-dimensional SRC nozzle is more uniform in the circumferential direction than that of the three-dimensional SRC. The CTEs of the three-dimensional/four-dimensional SRC show the isotropy and transverse isotropy about the nozzle axis. Because of this isotropy of the three-dimensional/four-dimensional SRC, the deformed shapes of the three-dimensional/four-dimensional SRC nozzle show almost uniform deformation in the circumferential direction.

However, as shown in Table 5, small irregular deformations of the three-dimensional SRC in circumferential direction in comparison with that of the four-dimensional SRC are caused by the mechanical properties rather than the thermal properties of the three-dimensional SRC. The maximum deformation of the three-dimensional SRC nozzle under the thermal and pressure loading is about 25 times greater than that under pressure loading only, which shows that most deformation of the nozzle is caused by thermal loading.

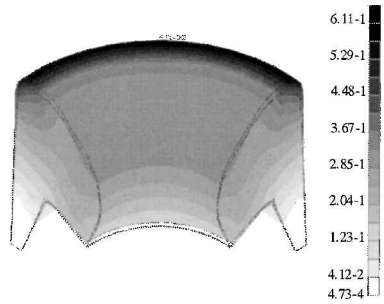

Three-dimensional SRC [1, 1, 1], mm, front view

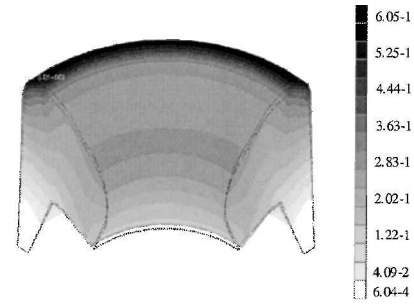

Four-dimensional SRC [1, 1, 1, 1], mm, front view

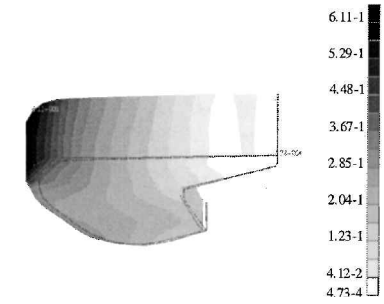

Three-dimensional SRC [1, 1, 1], mm, side view

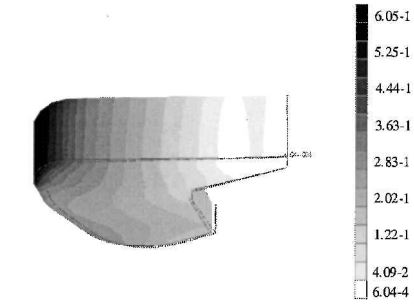

Four-dimensional SRC [1, 1, 1, 1], mm, side view

Fig. 17 Deformed shapes of the three-dimensional/four-dimensional SRC nozzles under pressure and thermal loading.

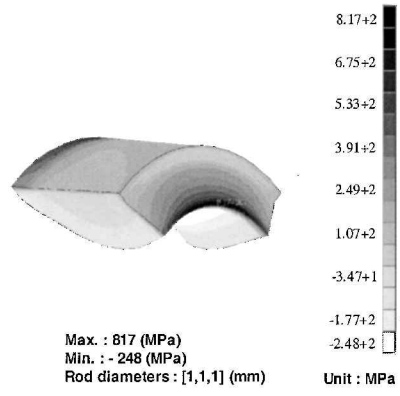

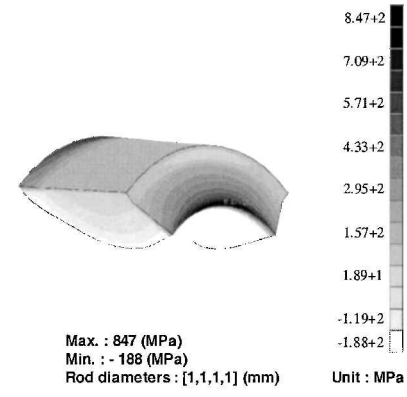

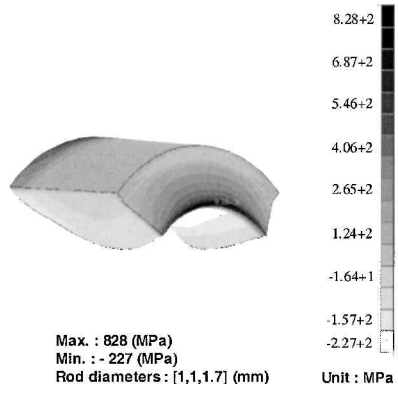

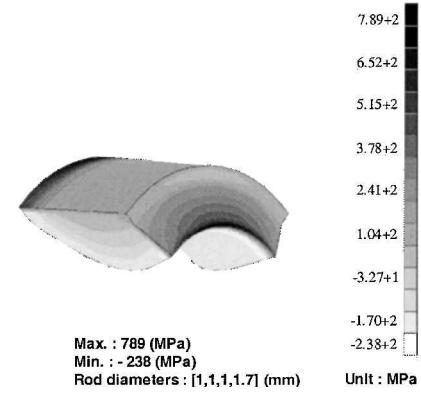

Fig. 18 Stress distribution of the several SRC nozzles in the circumferential direction.

The circumferential stress distributions of the three-dimensional/four-dimensional SRC nozzle, which are the most critical stress components among other stress components, are shown in Fig. 18. Most nozzle structures have a thermal expansion gap between each connecting part. The circumferential stress at connecting parts is much greater than the strength of SRC and carbon/phenolic because this thermal expansion gap was not considered in this study. The results indicate the importance of the thermal expansion gap. Among several three-dimensional/four-dimensional SRC nozzles, the four-dimensional SRC nozzle having diameters of [1,1,1,1.7 mm] in each rod direction has the smallest circumferential stress.

IV. Conclusions

The present study demonstrates how material properties of three- and four-dimensional SRCs can be predicted in all directions using volume average methods. For the three-dimensional SRC

considered herein, Young's modulus has the smallest value in the 45-deg rotated direction from each rod. The thermal conductivity and the CTE of the three-dimensional SRC, having the same rod diameter in each direction, exhibit isotropic behavior. For the four-dimensional SRC considered herein, Young's modulus has a constant value in the 1–2 plane due to quasi isotropy in the 1–2 plane. The tensile modulus has the smallest value in the 45-deg rotated direction from the 1–2 plane. The thermal conductivity and the CTE of the four-dimensional SRC, having the same rod diameter in each direction, display transverse isotropy.

The mechanical and thermal behavior of a kick motor nozzle incorporating several three-dimensional and four-dimensional SRCs are analyzed. The thermal gradient in the SRC nozzle in each connecting part causes high stress. The thermal loading is shown to have a greater effect on the deformation of the kick motor nozzle than the mechanical loading. Finally, the deformation of the four-dimensional SRC nozzle under thermal and pressure loading is slightly smaller and more uniform than the three-dimensional SRC nozzle. Also, the four-dimensional SRC nozzle having diameters of [1,1,1,1.7 mm] in each direction has the smallest circumferential stress among the several SRC nozzles.

References

[1]Byun, J.-H., Whitney, T. J., Du, G. W., and Chou, T. W., "Analytical Characterization of Two-Step Braided Composites," *Journal of Composite Materials*, Vol. 25, No. 12, 1991, pp. 1599–1618.

[2]Byun, J.-H., "Prediction of Engineering Constants for Plain and 8-Harness Satin Woven Composites," *Journal of The Korean Society of Mechanical Engineers (A)*, Vol. 21, No. 11, 1997, pp. 1757–1764.

[3]Rajiv, A. N., "Failure Analysis of Woven and Braided Fabric Reinforced Composites," *Journal of Composite Materials*, Vol. 29, No. 17, 1995, pp. 2334–2363.

[4]Rajiv, A. N., Peter, G. I., and John, E. M., "Effect of Fiber Architecture Parameters on Deformation Fields and Elastic Moduli of 2-D Braided Composites," *Journal of Composite Materials*, Vol. 28, No. 7, 1994, pp. 656–681.

[5]Neyfeh, A. H., and Hefzy, M. S., "Continuum Modeling of Three-Dimensional Trusslike Space Structures," *AIAA Journal*, Vol. 16, No. 8, 1978, pp. 779–787.

[6]Neyfeh, A. H., and Hefzy, M. S., "Continuum Modeling of the Mechanical and Thermal Behavior of Discrete Large Structures," *AIAA Journal*, Vol. 19, No. 6, 1981, pp. 766–773.

[7]Tai, H., "Equivalent Thermal Conductivity of Two- and Three-Dimensional Orthogonally Fiber-Reinforced Composites in One-Dimensional Heat Flow," *Journal of Composites Technology and Research*, Vol. 18, No. 3, 1996, pp. 221–227.

[8]Hashin, Z., "Analysis of Properties of Fiber Composites with Anisotropic Constituents," *Journal of Applied Mechanics*, Vol. 46, No. 3, 1979, pp. 543–550.

[9]Teters, G., and Kregers, A., "Effective Thermal Properties of Spatially Reinforced Fibrous Composite Materials," *Proceedings of the Second Baltic Heat Transfer Conference*, Riga, Latvia, 1995, pp. 493–502.

[10]Mukherjee, N., and Sinha, P. K., "Thermostructural Analysis of Rotationally Symmetric Multidirectional Fibrous Composite Structures," *Computers and Structures*, Vol. 65, No. 6, 1997, pp. 809–817.

[11]Yoo, J.-S., Lee, S.-E., and Kim, C.-G., "Prediction of Mechanical Behavior of Spatially Reinforced Composites for Kick Motor Nozzle," *Composite Structures*, Vol. 54, No. 1, 2001, pp. 57–65.

[12]Schmidt, D. L., Davidson, K. E., and Theibert, L. S., "Unique Applications of Carbon–Carbon Composite Materials," *SAMPE Journal*, Vol. 35, No. 4, 1999, pp. 51–63.

[13]Chamis, C. C., "Simplified Composite Micromechanics Equations for Hygral, Thermal, and Mechanical Properties," *SAMPE Quarterly*, April 1984, pp. 14–23.

[14]Kregers, A. F., "Mathematical Modeling of the Thermal Expansion of Spatially Reinforced Composites," *Mechanics of Composite Materials*, Vol. 24, No. 3, 1998, pp. 316–325.

[15]Dasgupta, A., and Agarwal, R. K., "Orthotropic Thermal Conductivity of Plain-weave Fabric Composites Using a Homegenization Technique," *Journal of Composite Materials*, Vol. 26, No. 18, 1992, pp. 2736–2758.

[16]*Engineered Materials Handbook*, desk ed., American Society for Materials International, Materials Park, OH, 1995, pp. 494–500.

[17]*Metals Handbook*, *Properties and Selection: Irons, Steels, and High-Performance Alloys*, 10th ed., Vol. 1, American Society for Materials International, Materials Park, OH, 1990, pp. 1–199.

M. S. Lake
Associate Editor